$\gamma\gamma$ and γp Events at High Energies*

Gerhard A. Schuler and Torbjörn Sjöstrand
Theory Division, CERN
CH-1211 Geneva 23
Switzerland

Abstract

A real photon has a complicated nature, whereby it may remain unresolved or fluctuate into a vector meson or a perturbative $q\overline{q}$ pair. Based on this picture, we previously presented a model for γp events that is based on the presence of three main event classes: direct, VMD and anomalous [1]. In $\gamma\gamma$ events, a natural generalization gives three-by-three combinations of the nature of the two incoming photons, and thus six distinct event classes. The properties of these classes are constrained by the choices already made, in the γp model, of cut-off procedures and other aspects. It is therefore possible to predict the energy-dependence of the cross section for each of the six components separately. The total cross section thus obtained is in good agreement with data, and also gives support to the idea that a simple factorized ansatz with a pomeron and a reggeon term can be a good approximation. Event properties undergo a logical evolution from pp to γp to $\gamma\gamma$ events, with larger charged multiplicity, more transverse energy flow and a higher jet rate in the latter process.

*Presented by T. Sjöstrand at the Workshop on Two-Photon Physics from DAΦNE to LEP200 and Beyond, Paris, France, 2–4 February 1994

CERN-TH.7193/94
March 1994

1 Introduction

There are many reasons for being interested in $\gamma\gamma$ physics. The process $e^+e^- \to e^+e^-\gamma\gamma \to e^+e^-X$ will be a main one at LEP 2 and future linear e^+e^- colliders. Therefore, $\gamma\gamma$ events are always going to give a non-negligible background to whatever other physics one is interested in. However, more importantly, the collision between two photons provides the richest spectrum of (leading-order) processes that is available for any choice of two incoming elementary particles. For instance, since the photon has a hadronic component, all of hadronic physics is contained as a subset of the possibilities. A correct description of the components of the total $\gamma\gamma$ cross section is therefore the ultimate challenge of 'minimum-bias' physics.

The study of $\gamma\gamma$ physics has a long history, and it is not our intention here to give a complete list of references. Many topics have been covered by the contributions to this and other workshops [2]. For the approach we are going to take, one important line of work is the subdivision of photon interactions by the nature of the photon [3]. Minijet phenomenology has attracted much attention in recent years [4].

However, none of these approaches attempts to give a complete description of $\gamma\gamma$ cross sections and event properties, but only concentrate on specific topics. Here we will try to be more ambitious, and really provide all the necessary aspects in one single framework. The starting point is our model for γp physics [1], which can be generalized in an (almost) minimal fashion. The results presented here are preliminary, in the sense that a number of further cross-checks are in progress [5].

One main area is still left out of our description: in all that follows, both incoming photons are assumed to be on the mass shell. Further issues need to be addressed when either photon or both of them are virtual. For reasons of clarity, we also restrict ourselves to discussing what happens in the collision between two photons of given momenta. The addition of photon flux factors will complicate the picture, but not add anything fundamentally new.

2 Event Classes

To first approximation, the photon is a point-like particle. However, quantum mechanically, it may fluctuate into a (charged) fermion–antifermion pair. The fluctuations $\gamma \leftrightarrow q\overline{q}$ are of special interest to us, since such fluctuations can interact strongly and therefore turn out to be responsible for the major part of the γp and $\gamma\gamma$ total cross sections, as we shall see. On the other hand, the fluctuations into a lepton pair are uninteresting, since such states do not undergo strong interactions to leading order, and therefore contribute negligibly to total hadronic cross sections. The leptonic fluctuations are perturbatively calculable, with an infrared cut-off provided by the lepton mass itself. Not so for quark pairs, where low-virtuality fluctuations enter a domain of non-perturbative QCD physics. It is therefore customary to split the spectrum of fluctuations into a low-virtuality and a high-virtuality part. The former part can be approximated by a sum over low-mass vector-meson states, customarily (but not necessarily) restricted to the lowest-lying vector multiplet. Phenomenologically, this Vector Meson Dominance (VMD) ansatz turns out to be very successful in describing a host of data. The high-virtuality part, on the other hand, should be in a perturbatively calculable domain.

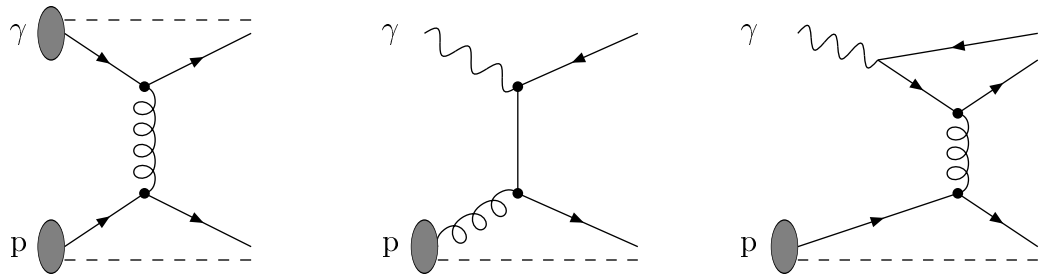

Figure 1: Contributions to hard γp interactions: a) VMD, b) direct, and c) anomalous. Only the basic graphs are illustrated; additional partonic activity is allowed in all three processes. The presence of spectator jets has been indicated by dashed lines, while full lines show partons that (may) give rise to high-$p_\perp$ jets.

In total, the photon wave function can then be written as

$$|\gamma\rangle = c_{\rm bare}|\gamma_{\rm bare}\rangle + \sum_{V=\rho^0,\omega,\phi,{\rm J}/\psi} c_V|V\rangle + \sum_{\rm q={\rm u,d,s,c,b}} c_{\rm q}|{\rm q\overline{q}}\rangle + \sum_{\ell={\rm e},\mu,\tau} c_\ell|\ell^+\ell^-\rangle \qquad (1)$$

(neglecting the small contribution from Υ). In general, the coefficients c_i depend on the scale μ used to probe the photon. Thus $c_\ell^2 \approx (\alpha_{\rm em}/2\pi)(2/3)\ln(\mu^2/m_\ell^2)$. Introducing a cut-off parameter p_0 to separate the low- and high-virtuality parts of the q$\overline{\rm q}$ fluctuations, one similarly obtains $c_{\rm q}^2 \approx (\alpha_{\rm em}/2\pi)2e_{\rm q}^2\ln(\mu^2/p_0^2)$. The VMD part corresponds to the range of q$\overline{\rm q}$ fluctuations below p_0 and is thus μ-independent (assuming $\mu > p_0$). In conventional notation $c_V^2 = 4\pi\alpha_{\rm em}/f_V^2$, with $f_V^2/4\pi$ determined from data to be 2.20 for ρ^0, 23.6 for ω, 18.4 for ϕ and 11.5 for J/ψ [6]. Finally, $c_{\rm bare}$ is given by unitarity: $c_{\rm bare}^2 \equiv Z_3 = 1 - \sum c_V^2 - \sum c_{\rm q}^2 - \sum c_\ell^2$. In practice, $c_{\rm bare}$ is always close to unity. Usually the probing scale μ is taken to be the transverse momentum of a $2 \to 2$ parton-level process. Our fitted value $p_0 \approx 0.5$ GeV (see below) then sets the minimum transverse momentum of a perturbative branching $\gamma \to$ q$\overline{\rm q}$.

The subdivision of the above photon wave function corresponds to the existence of three main event classes in γp events, cf. Fig. 1:

1. The VMD processes, where the photon turns into a vector meson before the interaction, and therefore all processes allowed in hadronic physics may occur. This includes elastic and diffractive scattering as well as low-$p_\perp$ and high-$p_\perp$ non-diffractive events.
2. The direct processes, where a bare photon interacts with a parton from the proton.
3. The anomalous processes, where the photon perturbatively branches into a q$\overline{\rm q}$ pair, and one of these (or a daughter parton thereof) interacts with a parton from the proton.

All three processes are of $O(\alpha_{\rm em})$. However, in the direct contribution the photon structure function is of $O(1)$ and the hard scattering matrix elements of $O(\alpha_{\rm em})$, while the opposite holds for the VMD and the anomalous processes. As we already noted, the $\ell^+\ell^-$ fluctuations are not interesting, and there is thus no class associated with them.

The above subdivision is not unique, or even the conventional one. More common is to lump the jet production processes of VMD and anomalous into a class called resolved photons. The remaining 'soft-VMD' class is then defined as not having any jet production at all, but only consisting of low-$p_\perp$ events. We find such a subdivision counterproductive, since it is then not possible to think of the VMD class as being a scaled-down version (by a factor c_V^2) of ordinary hadronic processes — remember that normal hadronic collisions *do* contain jets part of the time.

In a complete framework, there would be no sharp borders between the three above classes, but rather fairly smooth transition regions that interpolate between the extreme behaviours. However, at our current level of understanding, we do not know how to do this, and therefore push our ignorance into parameters such as the p_0 scale and the $f_V^2/4\pi$ couplings. From a practical point of view, the sharp borders on the parton level are smeared out by parton showers and hadronization. Any Monte Carlo event sample intended to catch a border region would actually consist of a mixture of the three extreme scenarios, and therefore indeed be intermediate. Also, remember that our separation is applied to leading-order processes, with higher-order effects included only in the leading-logarithmic approximation. An additional scheme dependence would arise for truly higher-order matrix elements.

The difference between the three classes is easily seen in terms of the beam jet structure. The incoming proton always gives a beam jet containing the partons of the proton that did not interact. On the photon side, the direct processes do not give a beam jet at all, since all the energy of the photon is involved in the hard interaction. The VMD ones (leaving aside the elastic and diffractive subprocesses for the moment) give a beam remnant just like the proton, with a 'primordial $k_\perp$' smearing of typically up to half a GeV. The anomalous processes give a beam remnant produced by the $\gamma \to \mathrm{q\overline{q}}$ branching, with a transverse momentum going from p_0 upwards. Thus the transition from VMD to anomalous should be rather smooth.

A generalization of the above picture to $\gamma\gamma$ events is obtained by noting that each of the two incoming photons is described by a wave function of the type given in eq. (1). In total, there are therefore three times three event classes. By symmetry, the 'off-diagonal' combinations appear pairwise, so the number of distinct classes is only six. These are, cf. Fig. 2:

1. VMD×VMD: both photons turn into hadrons, and the processes are therefore the same as allowed in hadron–hadron collisions.
2. VMD×direct: a bare photon interacts with the partons of the VMD photon.
3. VMD×anomalous: the anomalous photon perturbatively branches into a $\mathrm{q\overline{q}}$ pair, and one of these (or a daughter parton thereof) interacts with a parton from the VMD photon.
4. Direct×direct: the two photons directly give a quark pair, $\gamma\gamma \to \mathrm{q\overline{q}}$. Also lepton pair production is allowed, $\gamma\gamma \to \ell^+\ell^-$, but will not be considered by us.
5. Direct×anomalous: the anomalous photon perturbatively branches into a $\mathrm{q\overline{q}}$ pair, and one of these (or a daughter parton thereof) directly interacts with the other photon.
6. Anomalous×anomalous: both photons perturbatively branch into $\mathrm{q\overline{q}}$ pairs, and subsequently one parton from each photon undergoes a hard interaction.

The first three classes above are pretty much the same as the three classes allowed in γp events, since the interactions of a VMD photon and those of a proton are about

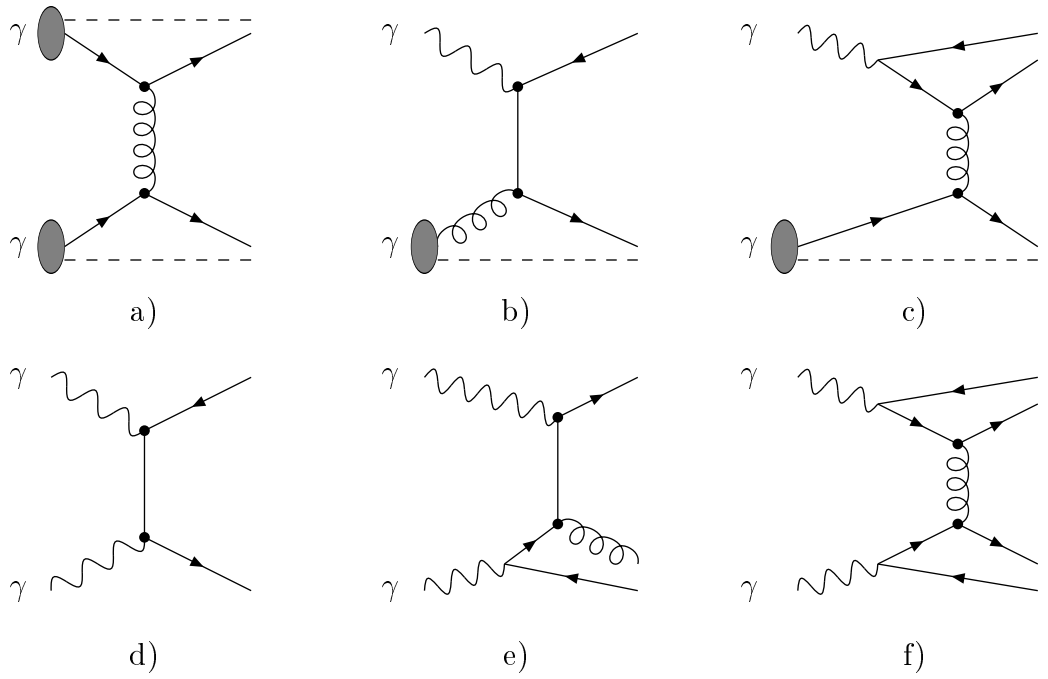

Figure 2: Contributions to hard $\gamma\gamma$ interactions: a) VMD×VMD, b) VMD×direct, c) VMD×anomalous, d) direct×direct, e) direct×anomalous, and f) anomalous×anomalous. Notation as in Fig. 1.

the same.

The main parton-level processes that occur in the above classes are:

- The 'direct' processes $\gamma\gamma \to \mathrm{q\overline{q}}$ only occur in class 4.
- The '1-resolved' processes $\gamma\mathrm{q} \to \mathrm{qg}$ and $\gamma\mathrm{g} \to \mathrm{q\overline{q}}$ occur in classes 2 and 5.
- The '2-resolved' processes $\mathrm{qq}' \to \mathrm{qq}'$ (where q' may also represent an antiquark), $\mathrm{q\overline{q}} \to \mathrm{q}'\overline{\mathrm{q}}'$, $\mathrm{q\overline{q}} \to \mathrm{gg}$, $\mathrm{qg} \to \mathrm{qg}$, $\mathrm{gg} \to \mathrm{q\overline{q}}$ and $\mathrm{gg} \to \mathrm{gg}$ occur in classes 1, 3 and 6.
- Elastic, diffractive and low-$p_\perp$ events occur in class 1.

The notation direct, 1-resolved and 2-resolved is the conventional subdivision of $\gamma\gamma$ interactions. The rest is then called 'soft-VMD'. As for the γp case, our subdivision is an attempt to be more precise and internally consistent than the conventional classes allow. One aspect is that we really want to have a VMD×VMD class that is nothing but a scaled-down copy of the $\rho^0\rho^0$ and other vector-meson processes, with a consistent transition between low-$p_\perp$ and high-$p_\perp$ events (see below). Another aspect is that, in a complete description, the VMD and anomalous parts of the photon give rise to different beam remnant structures, as discussed above, even when the hard subprocess itself may be the same.

A third aspect is that our subdivision provides further constraints; these, at least in principle, make the model more predictive. In particular, the parton distributions of the photon are constrained by the ansatz in eq. (1) to be given by

$$f_a^\gamma(x,\mu^2) = f_a^{\gamma,\mathrm{dir}}(x,\mu^2) + f_a^{\gamma,\mathrm{VMD}}(x,\mu^2) + f_a^{\gamma,\mathrm{anom}}(x,\mu^2;p_0^2) \; . \tag{2}$$

Here

$$f_a^{\gamma,\mathrm{dir}}(x,\mu^2) = Z_3 \, \delta_{a\gamma} \, \delta(1-x) \tag{3}$$

and

$$f_a^{\gamma,\mathrm{VMD}}(x,\mu^2) = \sum_{V=\rho^0,\omega,\phi,\mathrm{J}/\psi} \frac{4\pi\alpha}{f_V^2} f_a^V(x,\mu^2) \; . \tag{4}$$

The anomalous part, finally, is fully calculable perturbatively, given the boundary condition that the distributions should vanish for $\mu^2 = p_0^2$. In principle, everything is therefore given. In practice, the vector-meson distributions are not known, and so one is obliged to make further assumptions, such as $\rho^0 \approx \pi^0 \approx (\pi^+ + \pi^-)/2$. Since the ρ^0 is rather short-lived, it is not impossible that it could be somewhat different from a π, e.g. with fewer partons at small x. By comparison, conventional distributions are defined for resolved processes only:

$$f_a^{\gamma,\mathrm{res}}(x,\mu^2) = f_a^{\gamma,\mathrm{VMD}}(x,\mu^2) + f_a^{\gamma,\mathrm{anom}}(x,\mu^2;p_0^2) \; . \tag{5}$$

The resolved distributions are then assumed to be given in a completely free way, at some input scale, i.e. without any direct relation with the vector-meson distributions.

3 Cross Sections

Total hadronic cross sections show a characteristic fall-off at low energies and a slow rise at higher energies. This behaviour can be parametrized by the form

$$\sigma_{\mathrm{tot}}^{AB}(s) = X^{AB} s^{\epsilon} + Y^{AB} s^{-\eta} \tag{6}$$

for $A + B \to X$. The powers ϵ and η are universal, with fit values [7]

$$\epsilon \approx 0.0808 \; , \qquad \eta \approx 0.4525 \; , \tag{7}$$

while the coefficients X^{AB} and Y^{AB} are process-dependent. Equation (6) can be interpreted within Regge theory, where the first term corresponds to pomeron exchange and gives the asymptotic rise of the cross section. Ultimately, this increase violates the Froissart–Martin bound [8]; ϵ should therefore be thought of as slowly decreasing with energy (owing to multi-pomeron exchange effects), although data at current energies are well fitted by a constant ϵ. The second term, the reggeon one, is mainly of interest at low energies. For the purpose of our study we do not rely on the Regge interpretation of eq. (6), but can merely consider it as a convenient parametrization.

The VMD part of the γp cross section should have a similar behaviour, but there is no compelling reason why the direct and anomalous parts would have to. However, empirically, the γp data are well described by

$$\sigma_{\mathrm{tot}}^{\gamma\mathrm{p}}(s) \approx 67.7\, s^{\epsilon} + 129\, s^{-\eta} \;\; [\mu\mathrm{b}], \tag{8}$$

with s in GeV^2. (Cross-sections are throughout given in mb for hadron–hadron interactions, in μb for γ–hadron ones and in nb for $\gamma\gamma$ ones.) Actually, the above formula is a prediction [7] preceding the HERA data [9].

If we take the Regge-theory ansatz seriously also for the photon, it is possible to derive an expression for the total $\gamma\gamma$ cross section

$$\sigma_{\mathrm{tot}}^{\gamma\gamma}(s) \approx 211\, s^{\epsilon} + 297\, s^{-\eta} \;\; [\mathrm{nb}]. \tag{9}$$

This is based on the assumption that the pomeron and reggeon terms factorize, $X^{AB} = \beta_{A\mathbb{P}}\beta_{B\mathbb{P}}$ and $Y^{AB} = \gamma_{A\mathbb{R}}\gamma_{B\mathbb{R}}$, so that $X^{\gamma\gamma} = (X^{\gamma\mathrm{p}})^2/X^{\mathrm{pp}}$ and $Y^{\gamma\gamma} = (Y^{\gamma\mathrm{p}})^2/Y^{\mathrm{pp}}$, with $X^{\mathrm{pp}} \approx 21.70$ and $Y^{\mathrm{pp}} \approx 56.08$. In hadronic cross sections, factorization seems valid for the pomeron term but not for the reggeon one, e.g. $X^{\overline{\mathrm{p}}\mathrm{p}} = X^{\mathrm{pp}}$ while $Y^{\overline{\mathrm{p}}\mathrm{p}} \approx 98.39 \gg Y^{\mathrm{pp}}$. An equally valid guess for $Y^{\gamma\gamma}$ would then be obtained by $Y^{\gamma\gamma} = 2(Y^{\gamma\mathrm{p}})^2/(Y^{\mathrm{pp}}+Y^{\overline{\mathrm{p}}\mathrm{p}}) \approx 215$. The uncertainty in $Y^{\gamma\gamma}$ only affects the low-energy behaviour, and so is not critical for us.

Note that factorization is assumed to hold separately for the pomeron and the reggeon terms, not for the total cross section itself. That is, the relation $\sigma_{\mathrm{tot}}^{\gamma\gamma} = (\sigma_{\mathrm{tot}}^{\gamma\mathrm{p}})^2/\sigma_{\mathrm{tot}}^{\mathrm{pp}}$ is not exact in this approach, although numerically it is a very good approximation.

Our eq. (9) above should be compared with the time-honoured expression $\sigma^{\gamma\gamma} = 240 + 270/W$ [10]. This corresponds to a critical pomeron, $\epsilon = 0$, as was commonly assumed in the early seventies, and an $\eta = 0.5$, but it is otherwise in the same spirit as our formula. Also numerically the two closely agree at not too large energies.

One should remember that our expression (9) is here 'derived' based on a simple Regge-theory ansatz that has no real validity for the photon. Next we will proceed to study the contributions of the individual event classes. The constraints that come from γp physics data then directly feed into constraints on the contribution from these classes and therefore on the total $\gamma\gamma$ cross section. At the end of the day we will therefore show that a cross section behaving roughly like eq. (9) should be a good approximation. In doing so, the properties of the event classes are also fixed, to a large extent.

Based on the subdivision into event classes, the total γp cross section may be written as

$$\sigma_{\mathrm{tot}}^{\gamma\mathrm{p}} = \sigma_{\mathrm{VMD}}^{\gamma\mathrm{p}} + \sigma_{\mathrm{dir}}^{\gamma\mathrm{p}} + \sigma_{\mathrm{anom}}^{\gamma\mathrm{p}} \tag{10}$$

and the total $\gamma\gamma$ one as

$$\sigma_{\mathrm{tot}}^{\gamma\gamma} = \sigma_{\mathrm{VMD}\times\mathrm{VMD}}^{\gamma\gamma} + 2\sigma_{\mathrm{VMD}\times\mathrm{dir}}^{\gamma\gamma} + 2\sigma_{\mathrm{VMD}\times\mathrm{anom}}^{\gamma\gamma} + \sigma_{\mathrm{dir}\times\mathrm{dir}}^{\gamma\gamma} + 2\sigma_{\mathrm{dir}\times\mathrm{anom}}^{\gamma\gamma} + \sigma_{\mathrm{anom}\times\mathrm{anom}}^{\gamma\gamma} \; . \tag{11}$$

Here we explicitly keep the factor of 2 for the off-diagonal terms, where the rôle of the two incoming photons may be interchanged.

The Vp cross sections may be parametrized as

$$\sigma_{\mathrm{tot}}^{\rho^0\mathrm{p}} \approx \sigma_{\mathrm{tot}}^{\omega\mathrm{p}} \approx \frac{1}{2}\left(\sigma_{\mathrm{tot}}^{\pi^+\mathrm{p}} + \sigma_{\mathrm{tot}}^{\pi^-\mathrm{p}}\right) \approx 13.63\, s^{\epsilon} + 31.79\, s^{-\eta} \;\; [\mathrm{mb}], \tag{12}$$

$$\sigma_{\mathrm{tot}}^{\phi\mathrm{p}} \approx \sigma_{\mathrm{tot}}^{\mathrm{K}^+\mathrm{p}} + \sigma_{\mathrm{tot}}^{\mathrm{K}^-\mathrm{p}} - \sigma_{\mathrm{tot}}^{\pi^-\mathrm{p}} \approx 10.01\, s^{\epsilon} - 1.51\, s^{-\eta} \;\; [\mathrm{mb}]. \tag{13}$$

(The J/ψp cross section is taken to be about a tenth of the ϕp one, with a large amount of uncertainty; it is included in the complete analysis but is neglected in our discussion here.) Again using factorization for the pomeron and reggeon terms separately, the total cross section for two vector mesons is

$$\sigma_{\mathrm{tot}}^{V_1V_2} \approx \frac{X^{\mathrm{p}V_1}X^{\mathrm{p}V_2}}{X^{\mathrm{pp}}}\, s^{\epsilon} + \frac{Y^{\mathrm{p}V_1}Y^{\mathrm{p}V_2}}{Y^{\mathrm{pp}}}\, s^{-\eta} \; . \tag{14}$$

For a description of VMD events, a further subdivision into elastic (el), diffractive (sd and dd for single and double diffractive) and non-diffractive (nd) events is required. Keeping only the simplest diffractive topologies, one may write

$$\sigma_{\mathrm{tot}}^{AB}(s) = \sigma_{\mathrm{el}}^{AB}(s) + \sigma_{\mathrm{sd(XB)}}^{AB}(s) + \sigma_{\mathrm{sd(AX)}}^{AB}(s) + \sigma_{\mathrm{dd}}^{AB}(s) + \sigma_{\mathrm{nd}}^{AB}(s) \; . \tag{15}$$

The elastic and diffractive cross sections for all required Vp and V_1V_2 processes have been calculated and parametrized in the context of our model presented in ref. [11]. The non-diffractive cross-section is then given by whatever is left. The $\sigma_{\rm nd}$ may be further subdivided into a low-$p_\perp$ and a high-$p_\perp$ class. Since the $2 \to 2$ parton–parton scattering cross sections are divergent in the limit $p_\perp \to 0$, some further care is needed for this classification. We expect the perturbative formulae to break down at small $p_\perp$, since an exchanged gluon with a large transverse wavelength $\lambda_\perp \sim 1/p_\perp$ cannot resolve the individual colour charges inside a hadron. The hadron being a net colour singlet, the effective coupling should therefore vanish in this limit. A parameter $p_{\perp\rm min}$ is introduced to describe the border down to which the perturbative expression is assumed to be valid [1]:

$$p_{\perp\rm min}(s) = p_{\perp\rm min}^{\rm VMD}(s) \approx 1.3 + 0.15\,\frac{\ln(E_{\rm cm}/200)}{\ln(900/200)} \;\; [\rm GeV]\;. \tag{16}$$

The jet rate above $p_{\perp\rm min}$ may still be large, in fact even larger than the total $\sigma_{\rm nd}$. It is therefore necessary to allow for the possibility of having several perturbative parton–parton interactions in one and the same event, i.e. to unitarize the jet emission probability. We do this using the formalism of ref. [12].

The total VMD cross sections are obtained as weighted sums of the allowed vector-meson states,

$$\sigma_{\rm VMD}^{\gamma\rm p} = \sum_V \frac{4\pi\alpha_{\rm em}}{f_V^2}\,\sigma_{\rm tot}^{V\rm p} \approx 53.4\,s^{\epsilon} + 115\,s^{-\eta} \;\; [\mu\rm b], \tag{17}$$

$$\sigma_{\rm VMD\times VMD}^{\gamma\gamma} = \sum_{V_1} \frac{4\pi\alpha_{\rm em}}{f_{V_1}^2} \sum_{V_2} \frac{4\pi\alpha_{\rm em}}{f_{V_2}^2}\,\sigma_{\rm tot}^{V_1V_2} \approx 131\,s^{\epsilon} + 236\,s^{-\eta} \;\; [\rm nb]. \tag{18}$$

In Fig. 3 we show the breakdown of $\sigma_{\rm VMD\times VMD}^{\gamma\gamma}$ by vector-meson combination. Obviously the $\rho^0\rho^0$ combination dominates. The same kind of formulae as above also apply for the subdivision into elastic, diffractive and non-diffractive events. This subdivision is shown in Fig. 4 for the sum of all meson combinations, which then mainly reflects the $\rho^0\rho^0$ composition.

Comparing eqs. (8) and (17), about 80% of the γp total cross section is seen to come from the VMD term. The remaining 20% is to be attributed to the direct and anomalous components. At small energies the anomalous part is negligible, and so the dependence of the direct cross section on p_0 can be used to determine this parameter. We obtain a value of $p_0 \approx 0.5$ GeV, which is consistent with the simple-minded answer $p_0 \approx m_\phi/2$, and also gives a reasonable $f_a^{\gamma,\rm res}(x,\mu^2)$ [1]. The anomalous process contains two cut-off parameters, the p_0 scale for the photon to branch to a perturbative $\rm q\overline{q}$ pair and a $p_{\perp\rm min}^{\rm anom}$ scale for one of the anomalous-photon partons to interact in a hard process. As a first guess, one might choose $p_{\perp\rm min}^{\rm anom}$ also to be given by eq. (16). However, this turns out to give a cross section increasing too rapidly.

Physically, it is understandable why hard processes should be more suppressed at small $p_\perp$ in anomalous processes than in VMD ones: the anomalous photon corresponds to a $\rm q\overline{q}$ pair of larger virtuality than a VMD one, and hence of smaller spatial extent. The best recipe for including this physics aspect is not well understood. Remembering that the anomalous cross section is the product (or, more precisely, the convolution) of the anomalous parton distributions and the hard partonic $2 \to 2$ scattering cross sections, one can, purely pragmatically, imagine two extreme procedures to weaken the too-strong rise of $\sigma_{\rm anom}^{\gamma\rm p}$: either reduce the partonic cross section

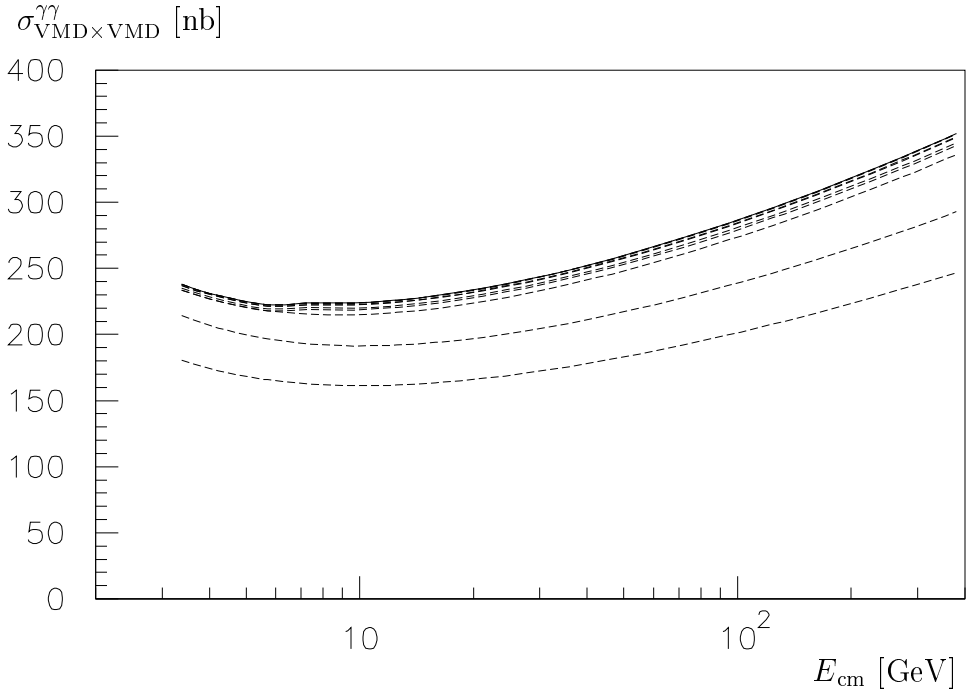

Figure 3: The total VMD×VMD cross section, full curve, and its subdivision by vector-meson combination. The components are separated by dashed curves, from bottom to top: $\rho^0\rho^0$, $\rho^0\omega$, $\rho^0\phi$, $\rho^0\mathrm{J}/\psi$, $\omega\omega$, $\omega\phi$, $\omega\mathrm{J}/\psi$, $\phi\phi$, $\phi\mathrm{J}/\psi$, and $\mathrm{J}/\psi\mathrm{J}/\psi$. Some of the latter components are too small to be resolved in the figure.

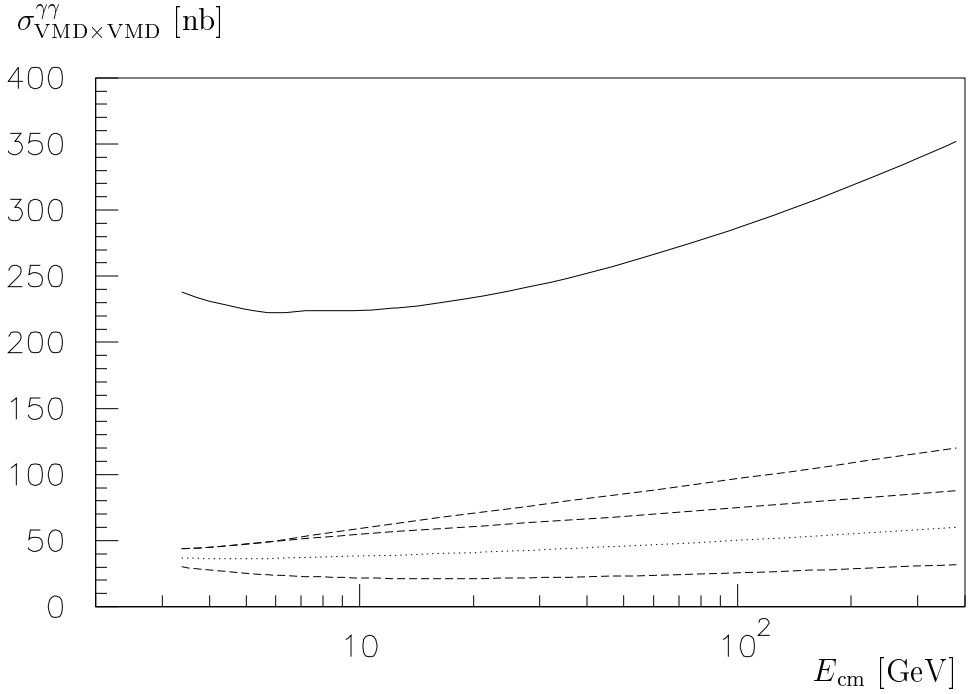

Figure 4: The total VMD×VMD cross section, full curve, and its subdivision by event topology. The components are separated by dashed curves, from bottom to top: elastic, single diffractive (split for the two sides by the dotted curve), double diffractive, and non-diffractive (including jet events unitarized).

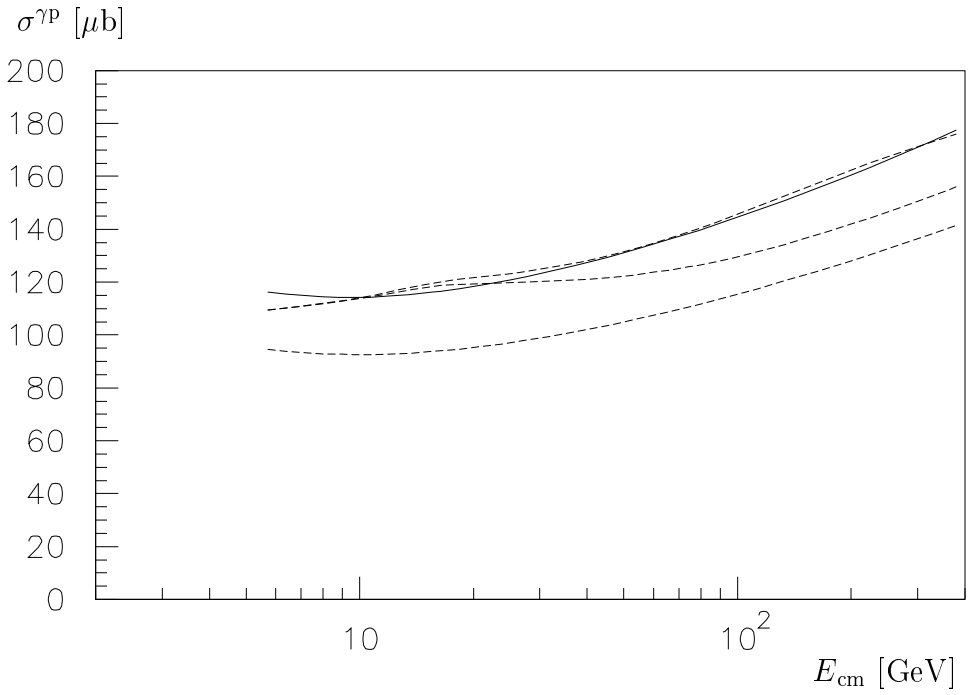

Figure 5: The total γp cross section and its subdivision by event topology. Full curve: the parametrization of eq. (8). The dashed curves, from bottom to top: VMD, VMD+direct and VMD+direct+anomalous.

by increasing $p_{\perp\min}^{\text{anom}}$, or decrease the values of the anomalous parton distributions by choosing a smaller value for the scale μ, compare eq. (2). Over the HERA energy range, say 100 GeV $\leq E_{\text{cm}} \leq$ 300 GeV, both choices

$$p_{\perp\min}^{\text{anom}}(s) = 1.5 + 0.0035\, E_{\text{cm}} \ \ [\text{GeV}] \qquad ; \qquad \mu = p_\perp \tag{19}$$

$$p_{\perp\min}^{\text{anom}}(s) = \qquad p_{\perp\min}^{\text{VMD}}(s) \qquad ; \qquad \mu = \frac{p_\perp}{r} \quad , \quad r \approx p_{\perp\min}^{\text{VMD}}/p_0 \tag{20}$$

give sensible answers, whereof we will use (19) as our main option. The resulting subdivision of the γp total cross section is shown in Fig. 5.

Turning to the $\gamma\gamma$ cross sections, in principle all free parameters have now been fixed, and the cross section for each of the six event classes can be obtained. The VMD$\times$VMD one has already been discussed; the others are given as integrals of $2 \to 2$ scattering cross sections above the respective $p_\perp$ cut-offs already specified. The results are shown in Fig. 6, class by class. For comparison, we also show the results that would be obtained if the simple factorization ansatz used to derive $\sigma_{\text{tot}}^{\gamma\gamma}$ in eq. (9) is valid component by component of the photon wave function. That is, if the composition of the γp cross section at some energy is 80% VMD, 15% direct and 5% anomalous, say, the $\gamma\gamma$ cross section is then assumed to be $0.8 \times 0.8 = 64\%$ VMD$\times$VMD, $2 \times 0.8 \times 0.15 = 24\%$ VMD$\times$direct, etc. This relative composition is then scaled by the assumed $\sigma_{\text{tot}}^{\gamma\gamma}$ of eq. (9) to get actual cross section numbers.

A few comments about each of the classes:

1. For the VMD$\times$VMD class in principle the simple factorization ansatz is exact in our model. The small deviations observed in Fig. 6a are not to be taken seriously, they come from the fact that the numerically integrated $\sigma_{\text{VMD}}^{\gamma\text{p}} + \sigma_{\text{dir}}^{\gamma\text{p}} + \sigma_{\text{anom}}^{\gamma\text{p}}$ does not agree perfectly with the desired $\sigma_{\text{tot}}^{\gamma\text{p}}$ of eq. (8), cf. Fig. 5. Therefore

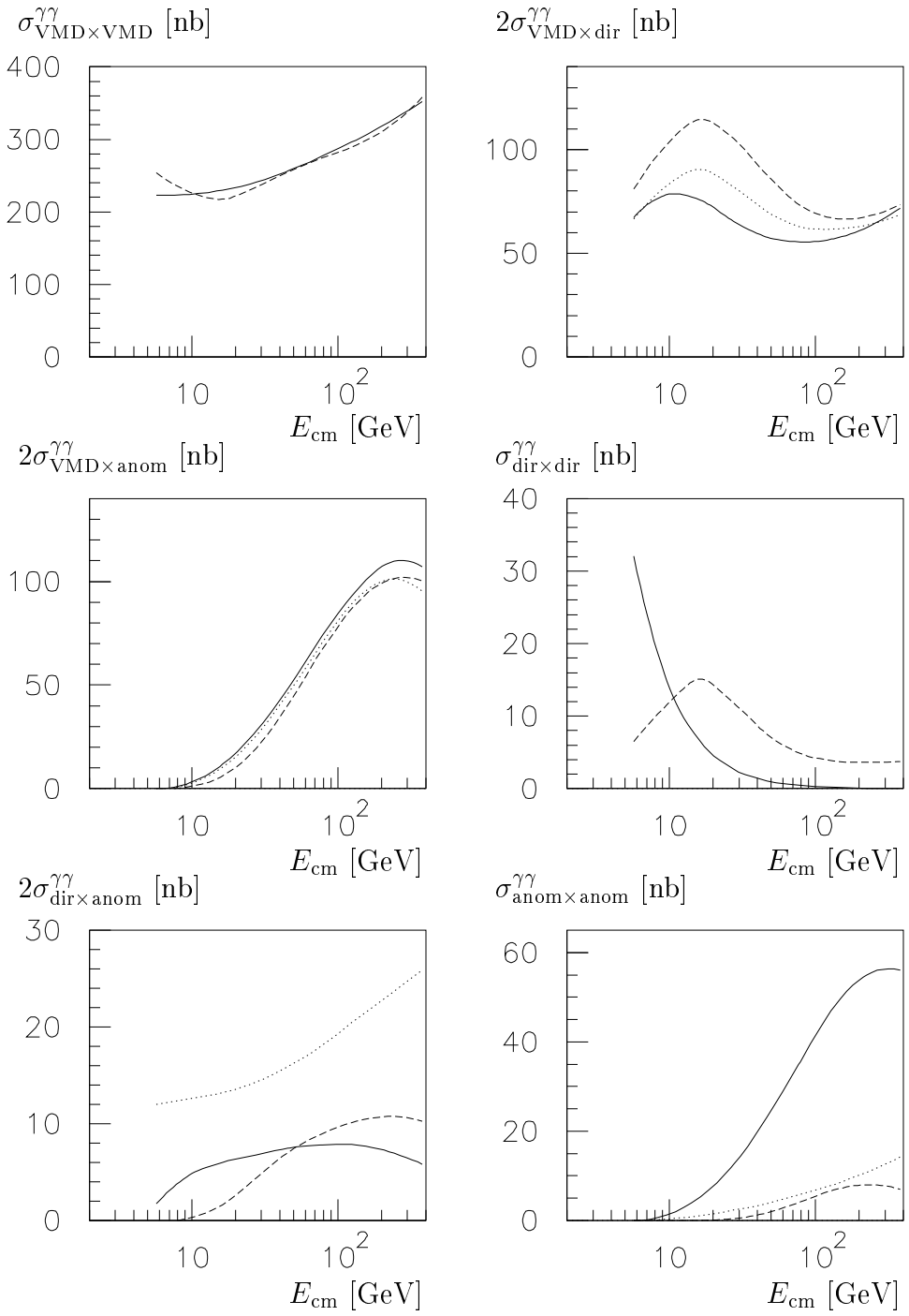

Figure 6: Comparison of $\gamma\gamma$ partial cross sections obtained by integration, full curves, and by a simple factorization ansatz, dashed curves. In a few of the plots, dotted curves give variations of the main curve obtained by integration, see text.

the relative γp composition used in the factorization ansatz has been slightly rescaled so as to add to unity.

2. Agreement is also acceptable for VMD$\times$direct. This is not so surprising, since this process is just a scaled-down version of a direct process on a vector meson target. Disagreements should therefore primarily come from differences between the meson and the proton structure functions. (The agreement would be perfect if the experimental input had come from $\rho^0\rho^0$ and $\gamma\rho^0$, and so forth for the other mesons, rather than from pp and γp.) We show an example of the variation that may come from using different sets of parton-distribution functions for the pion. The similarity of the large-energy behaviour reflects the fact that we have used the same small-x modification for both sets [1].
3. Also the VMD$\times$anomalous component agrees well; again this class can be seen as a scaled-down version of the anomalous γp class. The dependence on the choice of parton distributions is reduced, compared with the previous class, since anomalous processes involve larger x and μ^2 (i.e. better constrained regions) than the direct ones.
4. The direct$\times$direct component is not at all well predicted by the factorized ansatz. The latter yields a cross section growing at large energies at a rate related to the small-x behaviour of the proton distribution functions, i.e. $\propto s^{\epsilon}$ for our modified distributions. On the other hand, the total cross section for $\gamma\gamma \to \mathrm{q\overline{q}}$ is proportional to $\ln(s/p_0^2)/s$, and thus drops rapidly with c.m. energy. Charm production has here been included using massive matrix elements (whereas masses are neglected for a few other processes), since the assumed p_0 cut-off is smaller than the charm mass and since charm makes up a significant fraction of the total contribution.
5. The direct$\times$anomalous component again compares reasonably well with the prediction from factorization. There is some ambiguity about the choice of $p_\perp$ cut-off for hard scatterings, but it is seen that results are not drastically sensitive to this, even when the default $p_{\perp\mathrm{min}}^{\mathrm{anom}}$ cut-off of the hard process is replaced by p_0.
6. The anomalous$\times$anomalous process, finally, is most uncertain, because its cross section sensitively depends on the choice of method to keep $\sigma_{\mathrm{anom}}^{\gamma\mathrm{p}}$ low. Procedure (20) yields a much smaller cross section than (19), which is easily understood by recalling that $\mathrm{f}_a^{\gamma,\mathrm{anom}}$ enters quadratically in the anomalous$\times$anomalous cross section. If method (20) is the correct one then, in fact, factorization holds to a very good approximation. Also other mechanisms could be invoked to argue for a smaller $\sigma_{\mathrm{anom}\times\mathrm{anom}}^{\gamma\gamma}$ than the default one, such as the possibility of several parton–parton interactions in the same event.

When taking the sum of the six classes above, eq. (11), it should be remembered that the first three are the dominant ones. In fact, since the direct and anomalous components together give about 20% of the γp total cross section, the expectation is that the last three classes together would only give a 4% contribution to the total $\gamma\gamma$ cross section. Apart from the large uncertainty in the anomalous$\times$anomalous component, this is also the way it works out. The first three classes, on the other hand, are all related to the respective γp classes, with only a replacement of a p by a V (and an extra weight factor $4\pi\alpha_{\mathrm{em}}/f_V^2$). This makes the argumentation for eq. (9) credible, in spite of the absense of a (well-defined) coupling between a direct photon

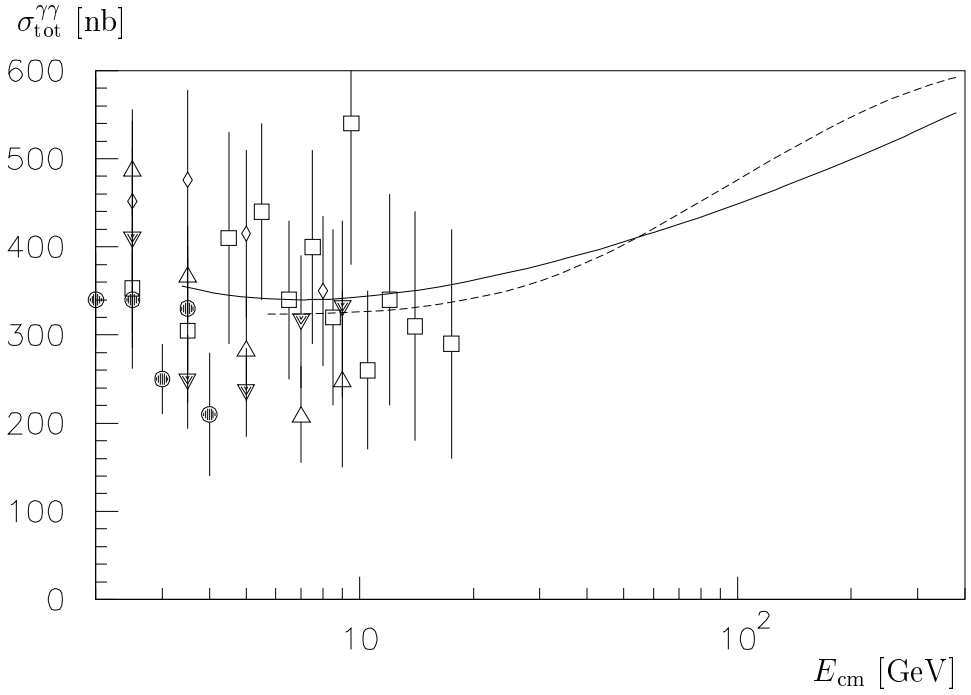

Figure 7: The total $\gamma\gamma$ cross section. Full curve: the parametrization of eq. (9). Dashed curve: result from sum of integrations of the six components. Data points: open triangles PLUTO 1984, filled triangles PLUTO 1986, squares TPC/2γ 1985, spades TPC/2γ 1991, circles MD-1 1991 [13].

and a pomeron.

The $\sigma_{\rm tot}^{\gamma\gamma}$ obtained by integration of the six components is compared with eq. (9) and experimental data in Fig. 7. As already discussed, the results of the integration are uncertain by some amount, so within this band of uncertainty the agreement with eq. (9) is very good. It is also readily seen that data are not (yet) precise enough to provide any real constraints, but are in generally good agreement with both approaches.

One can also compare our $\sigma_{\rm tot}^{\gamma\gamma}$ with the numbers obtained in various minijet-based approaches [4]. For $E_{\rm cm} = 200$ GeV, cross sections in the range 1000–1800 nb are typically obtained, but are reduced to about 500 nb if unitarity is enforced, in agreement with our results.

4 Event Properties

The subdivision of the total γp and $\gamma\gamma$ cross sections above, with the related choices of cut-off parameters etc., specifies the event composition at the hard-scattering level. For studies of the complete event structure, it is necessary to add models for initial- and final-state QCD radiation (parton showers), for beam remnants, and for fragmentation and secondary decays [1]. A Monte Carlo generation of complete hadronic final states is obtained with PYTHIA/JETSET [14]. Thus any experimental quantity can be studied. This section gives some representative examples. In particular, we compare the properties of pp, γp and $\gamma\gamma$ events. It should be noted that pp and $\overline{\rm p}$p events are very similar for the quantities studied here. Unless otherwise specified, the

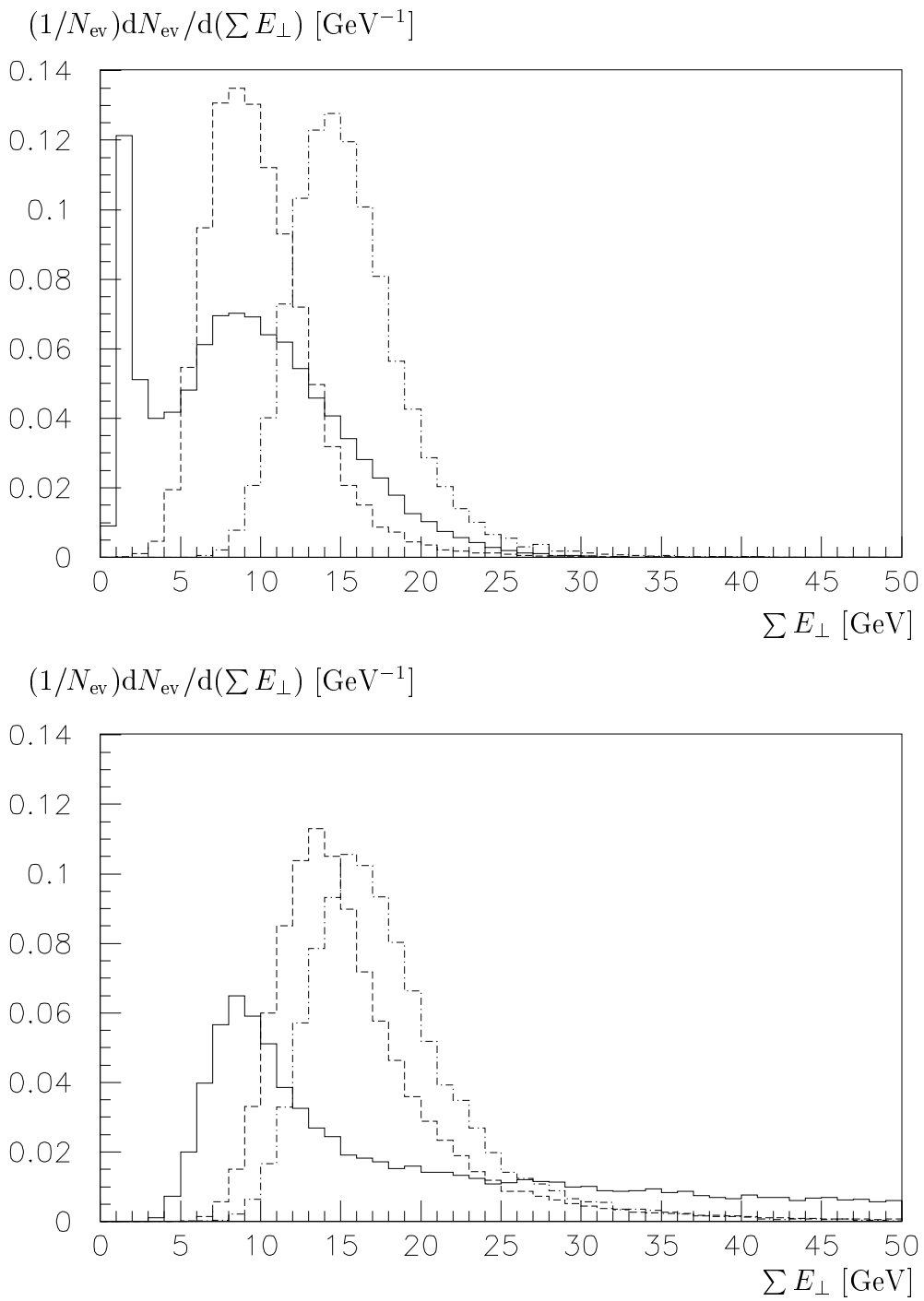

Figure 8: The total transverse energy per event, separately normalized for each of the six event classes. Top frame: VMD×VMD: full histogram; VMD×direct: dashed one; and VMD×anomalous: dash-dotted one. Bottom frame: direct×direct: full histogram; direct×anomalous: dashed one; and anomalous×anomalous: dash-dotted one.

figures refer to an $E_{\rm cm} = \sqrt{s_{\gamma\gamma}} = 100$ GeV. As we will show at the end of the section, the qualitative features do not depend critically on this choice.

Figure 8 shows the $\sum E_\perp$ per event for each of the six components of the $\gamma\gamma$ cross section. The spike at small $\sum E_\perp$ for the VMD×VMD class comes from elastic scattering events, e.g. $\gamma\gamma \to \rho^0\rho^0$. Also diffractive events contribute in this region. The

large-$\sum E_\perp$ tail of the VMD×VMD curve is enhanced by the possibility of multiple parton–parton interactions, which is only included for this class. Because of the larger $p_{\perp\min}^{\rm anom}$ cut-off, the classes involving anomalous photons typically have larger $\sum E_\perp$, while the smaller p_0 cut-off for the direct processes corresponds to smaller median $\sum E_\perp$. However, note that the $\gamma\gamma \to \mathrm{q\overline{q}}$ processes only fall off very slowly with $p_\perp$, in part because of the absense of structure functions, in part because of the form of the matrix element itself. The direct×direct class therefore wins out at very large $\sum E_\perp$.

The results of Fig. 8 are a bit misleading, since the relative importance of the six event classes is not visible. The weighted mixture is shown in Fig. 9, also compared with γp and pp events. One observes a steady progression, with $\langle \sum E_\perp \rangle_{\rm pp} < \langle \sum E_\perp \rangle_{\gamma\rm p} < \langle \sum E_\perp \rangle_{\gamma\gamma}$. This pattern, of more activity for a γ than for a p, is seen in essentially all distributions. The elastic spike at small $\sum E_\perp$ is less pronounced for $\gamma\gamma$, due to three factors: the VMD×VMD component is only a part of the $\gamma\gamma$ cross section, elastic scattering is a smaller fraction of the total $\rho^0\rho^0$ cross section than it is for pp, and kinetic energy in the $\rho^0 \to \pi^+\pi^-$ decays add to the total transverse energy.

The $E_\perp$ flow as a function of rapidity, $\mathrm{d}E_\perp/\mathrm{d}y$, is given in Fig. 10. It illustrates how γp interpolates between pp and $\gamma\gamma$: around the direction of the incoming photon, the γp events look like the $\gamma\gamma$ ones, while they look more like pp ones in the opposite direction, with an intermediate behaviour in the central region.

The charged-multiplicity distributions follow essentially the same pattern as shown for the $\sum E_\perp$ ones in Figs. 8, 9 and 10, and are therefore not included here. There is one noteworthy exception, however: the direct×direct component does not have a tail out to large multiplicities. That is, even if the process $\gamma\gamma \to \mathrm{q\overline{q}}$ can generate large $p_\perp$ values, the absence of any beam jets keeps the multiplicity down.

The transverse momentum spectrum of charged particles is shown in Fig. 11. The larger high-$p_\perp$ tail of the $\gamma\gamma$ processes is one of the simplest observables to experimentally establish differences between pp, γp and $\gamma\gamma$. Of course, the cause of the differences is to be sought in the higher jet rates associated with photon interactions. The jet spectra are compared in Fig. 12, using a simple cone algorithm where a minimum $E_\perp$ of 5 GeV is required inside a cone of $\Delta R = \sqrt{(\Delta\eta)^2 + (\Delta\phi)^2} < 1$. Already for an $E_{\perp\rm jet}$ of 5 GeV there are about ten times as many jets in $\gamma\gamma$ as in pp, and this ratio then increases with increasing $E_{\perp\rm jet}$.

To illustrate the energy dependence of these distributions, Figs. 13 and 14 give the $\mathrm{d}E_\perp/\mathrm{d}y$ flow for $\gamma\gamma$ c.m. energies of 25 and 400 GeV, respectively. These can be compared with the result for 100 GeV in Fig. 10. Qualitatively, the same pattern is seen at all three energies, although relative differences tend to be somewhat reduced at larger energies. This is also true for other observables, such as jet rates. One reason is that the possibility of multiple parton–parton interactions in the VMD component pushes up the activity in those events at larger energies, and thus brings them closer to the anomalous class. The importance of the direct class, on the other hand, is reduced at large energies. Further, at large energies, jet production is dominantly initiated by small-x incoming partons, where the VMD and anomalous distributions are more similar than at large x (although still different).

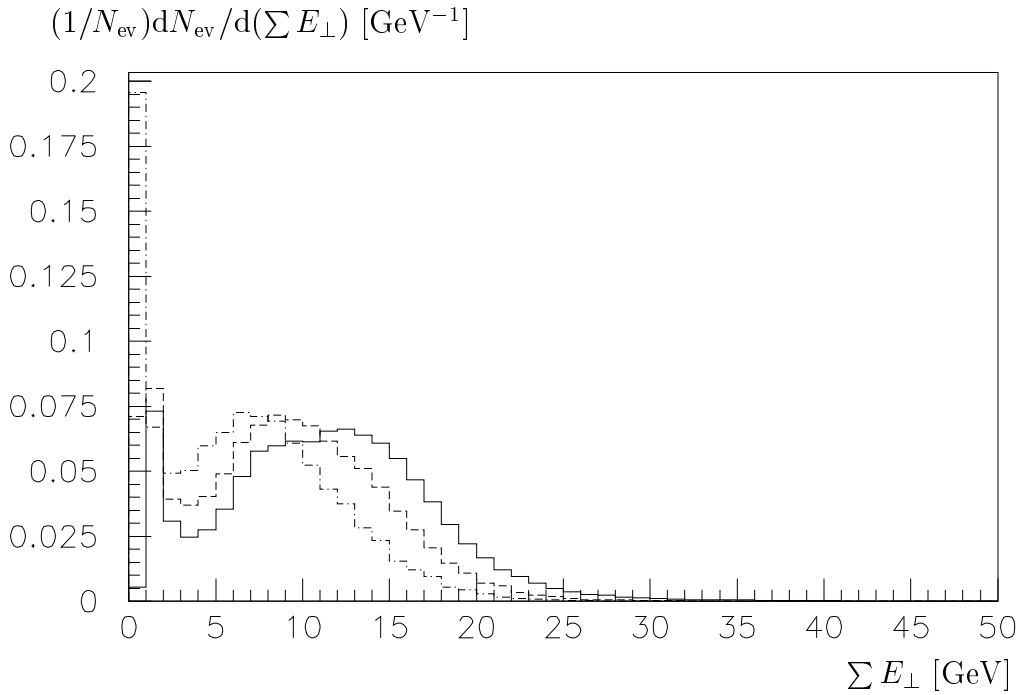

Figure 9: The total transverse energy per event for different beams: $\gamma\gamma$: full histogram; γp: dashed one: and pp: dash-dotted one.

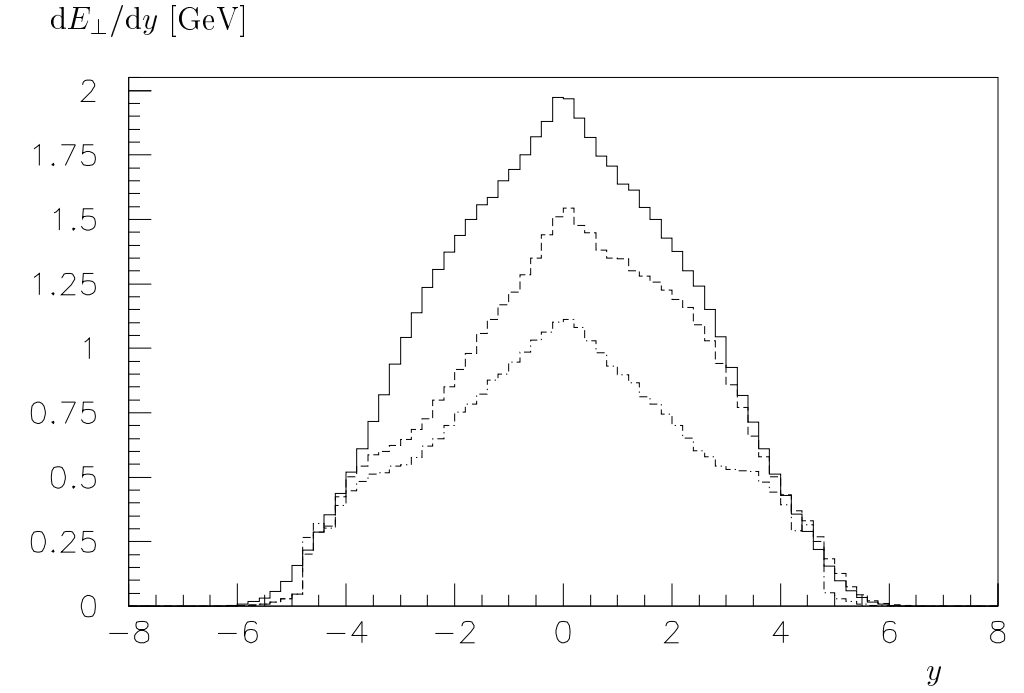

Figure 10: Transverse energy flow as a function of rapidity for different beams: $\gamma\gamma$: full histogram; γp: dashed one; and pp: dash-dotted one.

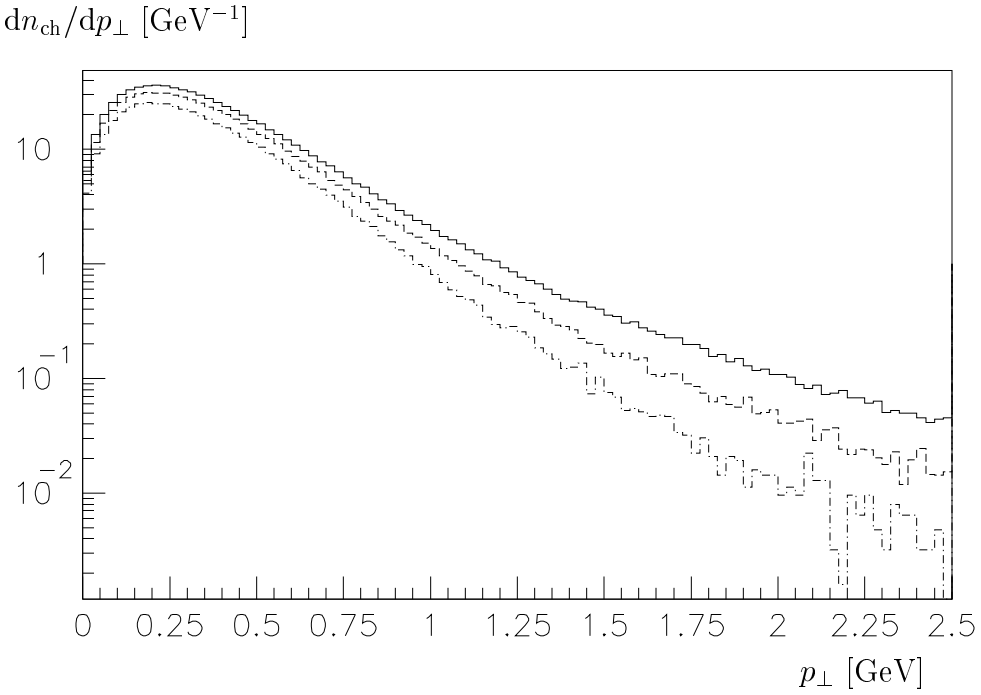

Figure 11: Charged particle inclusive $p_\perp$ spectra for different beams: $\gamma\gamma$: full histogram; γp: dashed one; and pp: dash-dotted one.

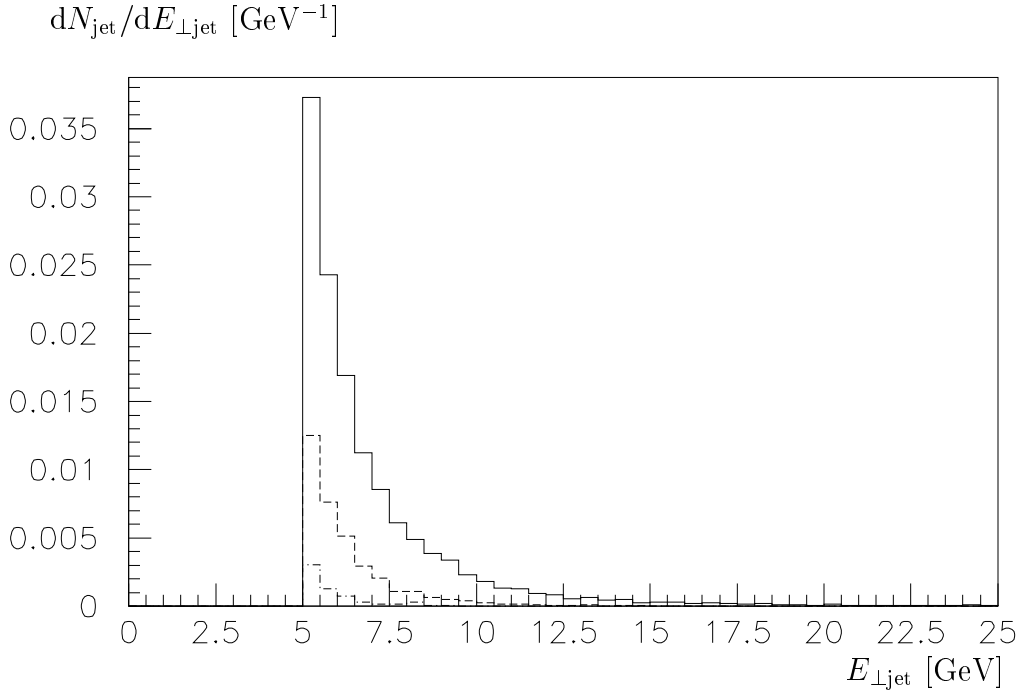

Figure 12: Jet rate as function of the transverse jet energy for different beams: $\gamma\gamma$: full histogram; γp: dashed one; and pp: dash-dotted one.

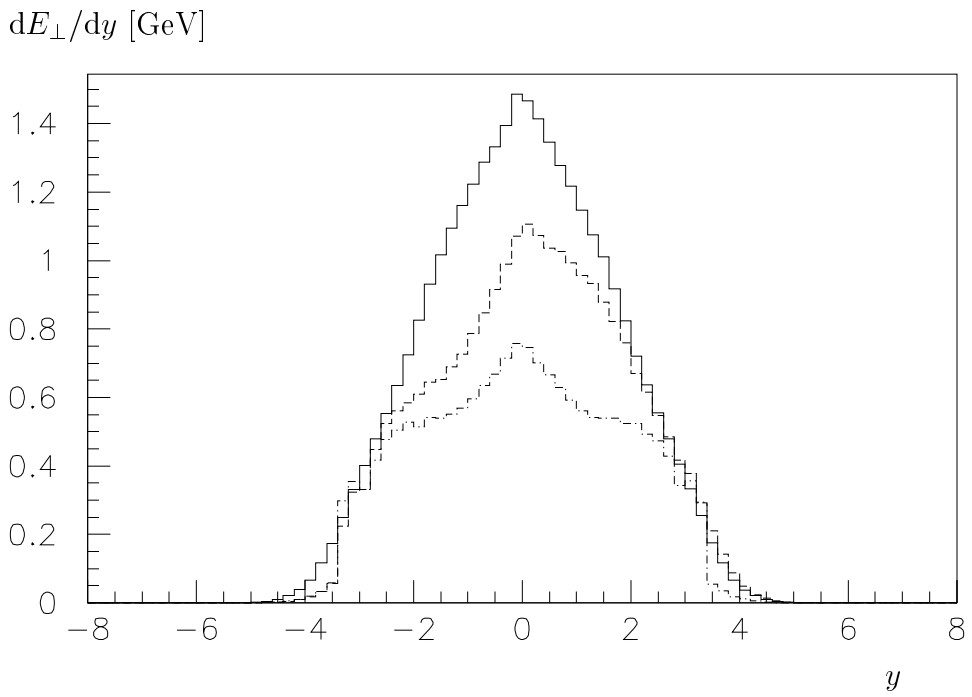

Figure 13: Transverse energy flow for $E_{\rm cm} = 25$ GeV as a function of rapidity for different beams: $\gamma\gamma$: full histogram; γp: dashed one; and pp: dash-dotted one.

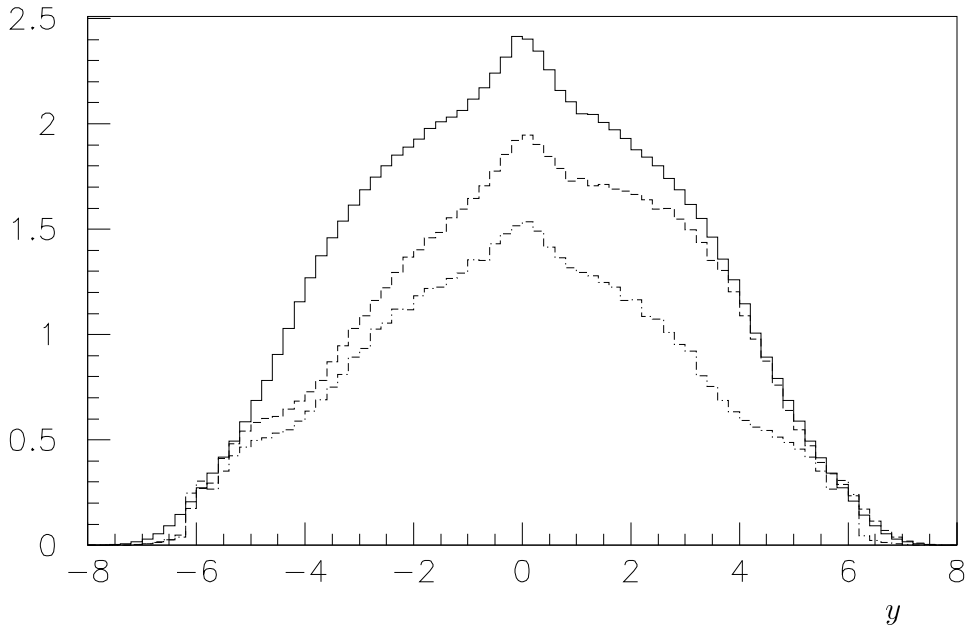

Figure 14: Transverse energy flow for $E_{\rm cm} = 400$ GeV as a function of rapidity for different beams: $\gamma\gamma$: full histogram; γp: dashed one; and pp: dash-dotted one.

5 Summary

In this paper we have shown that our model for γp events [1] can be consistently generalized to $\gamma\gamma$ events. That is, essentially all free parameters are fixed by (low-energy) γp phenomenology. Since we start out with a more detailed subdivision of the γp total cross section than has conventionally been done in the past, our $\gamma\gamma$ model also contains a richer spectrum of possible processes. We distinguish six main event classes, but most of these contain further subdivisions. The aim is that this approach will allow predictions for a broader range of observables than is addressed in conventional models. For instance, although not discussed in detail here, our approach does correlate the hard-jet physics in the central rapidity region with the structure of the beam remnants.

This does not mean that all results are complicated. We have shown that the simple Regge-theory expression $\sigma_{\mathrm{tot}}^{\gamma\gamma}(s) \approx 211\, s^{0.08} + 297\, s^{-0.45}$ [nb] comes very close to what is obtained in our full analysis. We therefore expect this expression to be good to better than 10% from a few GeV onwards, at least to the top $\gamma\gamma$ energies that could be addressed with the next generation of linear $\mathrm{e^+e^-}$ colliders. Also global event properties show a very simple pattern, with more activity (transverse energy, multiplicity, jets, ...) in γp events than in pp ones, and still more in $\gamma\gamma$ ones. This is perhaps contrary to the naïve image of a 'clean' point-like photon. The γp events show their intermediate status by having a photon (proton) hemisphere that looks much like $\gamma\gamma$ (pp) events, with a smooth interpolation in the middle.

This does not mean that all problems have been solved. In particular, the nature of the anomalous component of the photon is still not well understood. This is reflected in the different cut-off procedures that could be applied at small transverse momenta. Further, all the discussions so far have been on incoming real photons; the transition to the deeply-inelastic-scattering region has not been addressed so far. More problems may well crop up once our model is compared with observations. Therefore further data from HERA, TRISTAN, LEP 1 and 2, and future linear $\mathrm{e^+e^-}$ colliders will have much to teach us.

References

[1] G.A. Schuler and T. Sjöstrand, Phys. Lett. **B300** (1993) 169, Nucl. Phys. **B407** (1993) 539

[2] Proc. 8$^{\mathrm{th}}$ Int. Workshop on Photon–Photon Collisions, Shoresh, Israel, 1988, ed. U. Karshon (World Scientific, Singapore, 1988);
Proc. 9$^{\mathrm{th}}$ Int. Workshop on Photon–Photon Collisions, La Jolla, CA, USA, 1992, eds. D.O. Caldwell and H.P. Paar (World Scientific, Singapore, 1992)

[3] C. Peterson, T.F. Walsh and P.M. Zerwas, Nucl. Phys. **B229** (1983) 301;
J.H. Field, F. Kapusta and L. Poggioli, Z. Phys. **C36** (1987) 121;
P. Aurenche et al., Nucl. Phys. **B286** (1987) 553

[4] M. Drees and R.M. Godbole, Nucl. Phys. **B339** (1990) 355, Z. Phys. **C59** (1993) 591;
J.R. Forshaw and J.K. Storrow, Phys. Rev. **D46** (1992) 4955

[5] G.A. Schuler and T. Sjöstrand, in preparation

[6] T.H. Baur et al., Rev. Mod. Phys. **50** (1978) 261

[7] A. Donnachie and P.V. Landshoff, Phys. Lett. **B296** (1992) 227

[8] M. Froissart, Phys. Rev. **123** (1961) 1053;
A. Martin, Phys. Rev. **124** (1963) 1432

[9] ZEUS Collaboration, M. Derrick et al., Phys. Lett. **B293** (1992) 465;
H1 Collaboration, T. Ahmed et al., Phys. Lett. **B299** (1993) 374

[10] J.L. Rosner, in 'ISABELLE Physics Prospects', BNL Report 17522 (1972), p. 316

[11] G.A. Schuler and T. Sjöstrand, CERN-TH.6837/93, to appear in Phys. Rev. **D**

[12] T. Sjöstrand and M. van Zijl, Phys. Rev. **D36** (1987) 2019

[13] S.E. Baru et al., Z. Phys. **C53** (1992) 219, and references therein

[14] T. Sjöstrand and M. Bengtsson, Comput. Phys. Commun. **43** (1987) 367;
H.-U. Bengtsson and T. Sjöstrand, Comput. Phys. Commun. **46** (1987) 43;
T. Sjöstrand, CERN-TH.7111/93 and CERN-TH.7112/93